

Embedding semiclassical periodic orbits into chaotic many-body Hamiltonians

Andrew Hallam,¹ Jean-Yves Desaules,¹ and Zlatko Papić¹

¹*School of Physics and Astronomy, University of Leeds, Leeds LS2 9JT, UK*

Protecting coherent quantum dynamics from a chaotic environment is key to realizations of fragile many-body phenomena and their applications in quantum technology. We present a general construction that allows to embed a desired periodic orbit into a family of non-integrable many-body Hamiltonians, whose dynamics is otherwise chaotic. Our construction is based on time dependent variational principle that projects quantum dynamics onto a manifold of low-entangled states, and it generalizes the earlier approaches for embedding non-thermal eigenstates, known as quantum many-body scars, into thermalizing spectra. By designing terms that suppress “leakage” of the dynamics outside the variational manifold, we engineer families of Floquet models that host exact scarred dynamics, as we illustrate using a driven Affleck-Kennedy-Lieb-Tasaki model and a recent experimental realization of scars in a dimerized superconducting qubit chain.

Introduction.—The dynamics of non-integrable quantum many-body systems typically gives rise to rapid thermalization and scrambling of information. These hallmarks of quantum ergodicity can be traced to the properties of the system’s mid-spectrum eigenstates, which are generally highly entangled and obey the Eigenstate Thermalization Hypothesis (ETH) [1, 2]. In recent years, there has been a flurry of activity aimed at understanding the conditions for *weak* breaking of the ETH to emerge, in particular by devising ways of embedding non-thermalizing eigenstates into otherwise chaotic many-body spectra [3–5]. These eigenstates, referred to as quantum many-body scars (QMBSs), have been identified in prominent models of quantum magnets, such as the Affleck-Kennedy-Lieb-Tasaki (AKLT) model [6–8], and in Rydberg atom quantum simulators [9, 10], where their signatures were first observed in quench experiments [11]. Potential applications of QMBSs have been explored in the context of controlling quantum-information dynamics in complex systems [12] and for quantum metrology [13–15].

Despite much interest in weak ergodicity breaking phenomena in different experimental platforms [16–18], the origin of QMBSs remains the subject of ongoing investigation. In much of theoretical work, QMBSs are studied by algebraic constructions of ergodicity-breaking eigenstates. In particular, the local projector approach by Shiraishi and Mori [19] embeds a few non-thermal eigenstates into the spectrum of a non-integrable Hamiltonian. Other approaches construct families of eigenstates, representing condensates of quasiparticles that are evenly spaced in energy, through the repeated action of a quasiparticle creation operator on a selected initial state [8, 20]. More recent proposals aim to unify these different constructions into a single framework [21–24]. All these approaches, however, differ dramatically from the case of single-particle scars in quantum billiards, which are understood as quantum remnants of classical, unstable periodic orbits [25–28]. Nevertheless, for QMBSs observed in Rydberg atom experiments [11], the eigenstate constructions [10, 20, 29–31] were shown to be in

harmony with a semiclassical limit of the dynamics, developed by Ho *et al.* [32] by projecting quantum dynamics to a variational manifold spanned by states with low entanglement. The latter approach allows to identify a periodic orbit in the many-body Hilbert space that underpins QMBS dynamics, responsible for the strongly suppressed entanglement growth and coherent oscillations of expectation values of local observables.

In this work, we introduce a systematic method for embedding a desired periodic trajectory into the dynamics generated by a chaotic many-body Hamiltonian. To achieve this, we decompose the Hamiltonian into a component that generates an exact periodic orbit and a second component which vanishes upon taking the semiclassical limit. Thus, within a suitably-defined semiclassical manifold, the projected dynamics is a periodic oscillation. However, the dynamics of the full model may deviate from the projection to the manifold and this deviation is quantified by the so-called quantum leakage [32, 33]. Using the quantum leakage we introduce driving terms to the model that cancel the distinction between the semiclassical and quantum dynamics, schematically depicted in Fig. 1, which results in exact Floquet QMBSs. We demonstrate the utility of our approach using the AKLT model [6, 8] and a recent superconducting circuit realization of QMBS [18] based on the Su-Schrieffer-Heeger (SSH) model [34].

Time-dependent variational principle (TDVP).—To avoid the exponential complexity of many-body quantum systems, the TDVP method [35, 36] approximately solves the time-dependent Schrödinger equation (TDSE) by projecting it onto a manifold \mathcal{M} spanned by ansatz wave functions that capture the most important features of the dynamics. In this work we focus on one-dimensional lattice systems with a d -dimensional Hilbert space on each site, where \mathcal{M} is spanned by wave functions $|\psi(\{z_n\})\rangle$, parameterized by a complex variable z_n for each site n . For example, in a simple manifold describing product states of spins-1/2, one can think of z_n parameterizing the orientation of each spin on the Bloch sphere. However, as pointed out by Haegeman *et al.* [37], a much

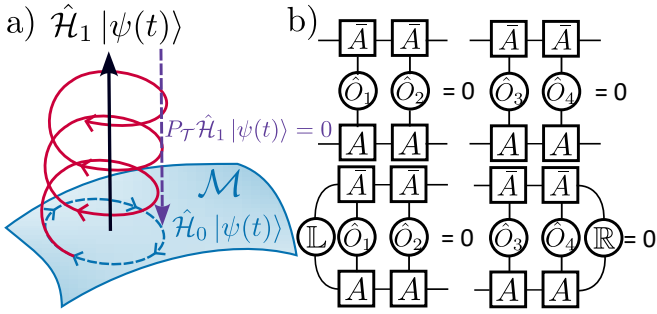


FIG. 1. (a) A periodic orbit can be embedded into a chaotic many-body Hamiltonian by decomposing the latter into two terms: $\hat{\mathcal{H}}_0$, which generates a periodic orbit in a semiclassical manifold \mathcal{M} , and $\hat{\mathcal{H}}_1$ that vanishes as the semiclassical limit is taken. (b) For an MPS manifold, $\hat{\mathcal{H}}_1$ takes a simplified form. The generic conditions for a four-site local $\hat{\mathcal{H}}_1$, valid for any system size and choice of boundary conditions, are illustrated. These conditions can be weakened for translation invariant MPS in the thermodynamic limit, as shown below.

larger class of dynamical behaviors can be described if we allow \mathcal{M} to contain some low-entangled states, which are conveniently represented by matrix product states (MPS) [38]. For MPS, the variables z_n on each site are different $\chi \times \chi$ dimensional matrices, A_n^s , $s = 1, 2, \dots, d$. Increasing χ increases the power of the ansatz, representing states with larger amounts of entanglement between sites.

The time evolution within \mathcal{M} is given by [36]

$$i \frac{d}{dt} |\psi(\{z_n\})\rangle = P_{\mathcal{T}(\{z_i\})} \hat{\mathcal{H}} |\psi(\{z_n\})\rangle, \quad (1)$$

where $P_{\mathcal{T}(\{z_i\})}$ is the projector onto the tangent-space of \mathcal{M} at the point $|\psi(\{z_n\})\rangle$:

$$P_{\mathcal{T}} = \sum_n |\partial_{z_n} \psi(\{z_n\})\rangle \langle \partial_{z_n} \bar{\psi}(\{\bar{z}_n\})|. \quad (2)$$

Due to the tangent-space projectors dependence on $\{z_n\}$, the TDVP dynamics typically deviate from that generated by the TDSE, becoming nonlinear. When \mathcal{M} is a so-called Kähler manifold, it is a classical dynamical phase space with the TDVP equations being the corresponding Hamilton equations [39, 40]. Additionally, when the states in \mathcal{M} form an overcomplete basis, a Feynman path integral over \mathcal{M} can be constructed [41]. The TDVP equations then correspond to the Euler-Lagrange equations of the path integral.

Semiclassical limit.—The deviation between TDVP and TDSE can be characterized using *quantum leakage* Γ [32]. The leakage is given by the norm of the difference between the two time-evolved wave functions, integrated around the orbit:

$$\Gamma = \frac{1}{T} \oint \|(\mathbb{1} - P_{\mathcal{T}}) \hat{\mathcal{H}} |\psi(\{z_n(t)\})\rangle\| dt. \quad (3)$$

Typically, Γ^2 is extensive, i.e., asymptotically proportional to the system size N . By constraining the complexity of \mathcal{M} , the TDVP approach allows one to effectively *define* a semiclassical limit of the full quantum dynamics [32]. Provided the full quantum dynamics are well-approximated within \mathcal{M} composed of low bond dimension MPS states, i.e., if $\Gamma \ll \sqrt{N}$, we will refer to such dynamics as “semiclassical”. Note that this definition admits the semiclassical limit to include (short-range) quantum correlations, which is essential, e.g., for capturing the behavior of constrained systems [32].

Orbit embedding conditions.—We now focus on Hamiltonians $\hat{\mathcal{H}}_0$ which possess a periodic orbit from a certain initial state, $|\psi(t)\rangle = |\psi(t+T)\rangle$, for which it is possible to find a low-dimensional \mathcal{M} which exactly captures the dynamics. Suppose the Hamiltonian is then perturbed, $\hat{\mathcal{H}}_0 \rightarrow \hat{\mathcal{H}}_0 + \hat{\mathcal{H}}_1$, so that the TDSE is altered, but Eq. (1) is not. A Hamiltonian that satisfies the following conditions along the trajectory will retain a semiclassical periodic orbit, despite its quantum dynamics being altered:

$$P_{\mathcal{T}} \hat{\mathcal{H}}_0 |\psi(\{z_n\})\rangle = \hat{\mathcal{H}}_0 |\psi(\{z_n\})\rangle, \quad (4)$$

$$\left[\hat{\mathcal{H}}_1 - \langle \bar{\psi}(\{\bar{z}_n\}) | \hat{\mathcal{H}}_1 |\psi(\{z_n\})\rangle \right] |\psi(\{z_n\})\rangle \neq 0, \quad (5)$$

$$P_{\mathcal{T}} \hat{\mathcal{H}}_1 |\psi(\{z_n\})\rangle = 0. \quad (6)$$

These conditions are illustrated in Fig. 1(a). Eq. (5) and Eq. (6) require that $|\psi(\{z_n\})\rangle$ is a fixed point of the TDVP equations with respect to $\hat{\mathcal{H}}_1$, while not being an eigenstate. For Hamiltonians that satisfy the conditions Eq. (4)-(6), the leakage can be simplified:

$$\Gamma = \frac{1}{T} \oint \|\hat{\mathcal{H}}_1 |\psi(\{z_n(t)\})\rangle\| dt. \quad (7)$$

Periodic orbit for MPS.—Restricting our discussion to MPS as a variational ansatz, we can be more precise about the form $\hat{\mathcal{H}}_1$ must take in order to satisfy Eq. (6). Suppose $\hat{\mathcal{H}}_1$ can be written as the tensor product of $2K$ -local operators

$$\hat{\mathcal{H}}_1 = \sum_n \bigotimes_{k=1}^{2K} \hat{O}_k^{n+k-1}. \quad (8)$$

For evaluating correlation functions with MPS, it is useful to introduce the MPS transfer matrix [42]:

$$\mathbb{E}_n(\hat{O}_k) = \sum_{s, \bar{s}'} \bar{A}_n^{s'} \hat{O}_{k,s,\bar{s}'}^n A_n^s. \quad (9)$$

In the Supplementary Material [43], we prove that Eq. (6) is satisfied for any system size and choice of boundary conditions if we impose:

$$\prod_{k=1}^K \mathbb{E}_{n+k-1}(\hat{O}_k) = 0, \quad \prod_{k=K+1}^{2K} \mathbb{E}_{n+k-1}(\hat{O}_k) = 0. \quad (10)$$

In the thermodynamic limit, these conditions can be significantly weakened. Let us assume that A_n^s is site-independent and $\mathbb{E}_n(\mathbb{1})$ possesses a unique dominant left and right eigenvector, $(\mathbb{L}|$ and $|\mathbb{R})$, respectively. In this case, Eq. (1) will always begin with $(\mathbb{L}|$ and end with $|\mathbb{R})$, so Eq. (6) is satisfied, provided

$$(\mathbb{L}| \prod_{k=1}^K \mathbb{E}_{n+k-1}(\hat{O}_k) = 0, \quad \prod_{k=K+1}^{2K} \mathbb{E}_{n+k-1}(\hat{O}_k) |\mathbb{R}) = 0. \quad (11)$$

These conditions are illustrated in Fig. 1(b) and below we demonstrate how they can be used to construct families of models that share the same periodic orbit, using SSH and AKLT chains as examples. We note that the form of $\hat{\mathcal{H}}_1$ in Eq. (8) was chosen for clarity but the generalization to Hamiltonians which are sums of local operators or feature long-range interactions is straightforward.

SSH chain.—We now apply our approach to the dimerized SSH model of polyacetylene [34],

$$\hat{\mathcal{H}}_{\text{SSH}} = \sum_{n=0}^{N/2-1} J_o \sigma_{2n+1}^+ \sigma_{2n+2}^- + \sum_{n=0}^{N/2-2} J_e \sigma_{2n+2}^+ \sigma_{2n+3}^- + \text{h.c.}, \quad (12)$$

where OBC have been assumed, σ^\pm denote the Pauli raising and lowering spin operators, and J_o and J_e are the hopping amplitudes on the odd and even sublattice, respectively. In Ref. [18], the SSH chain was used as a starting point to realize QMBS dynamics on a superconducting quantum processor when additional couplings between sites are added to break the integrability. In the absence of inter-dimer couplings, $J_e=0$, the state $|\psi(0)\rangle = |10011001\dots\rangle$, i.e., with dimers alternating between 10 and 01 local states, undergoes free precession, with frequency $2J_o$. The oscillations are no longer perfect at $J_e \approx 2J_o/3$ and instead exhibit a decaying envelope [18]. It was found that a translation invariant next-next nearest neighbor hopping enhances the QMBS oscillations. Indeed, as we show in [43], such a term reduces leakage from the scarred subspace, but it does not lead to its total suppression. However, using the above approach, we can identify a driving protocol that embeds an exact periodic trajectory into the model.

In order to embed the periodic trajectory into the SSH chain, we block together sites $\{2n, 2n+1\}$ and use a $d=4$, $\chi=1$ MPS ansatz. The SSH Hamiltonian in Eq. (12) then neatly fits into the form introduced above, with $\hat{\mathcal{H}}_0$ being the J_o term and $\hat{\mathcal{H}}_1$ the J_e term. It is straightforward to see that Eq. (5) is satisfied. To see that Eq. (6) is satisfied, we note that because the variational parameters are localized to a single site, each term in the sum defining $P_{\mathcal{T}}$ differs from $|\psi(t)\rangle$ on just one site. $\hat{\mathcal{H}}_1$ acting on $|\psi(t)\rangle$ makes it orthogonal to $|\psi(t)\rangle$ on two sites, therefore $\hat{\mathcal{H}}_1 |\psi(t)\rangle$ is annihilated by $P_{\mathcal{T}}$. In this sense, the SSH Hamiltonian for any J_e has the same semiclassical limit, corresponding to the quantum dynamics of the

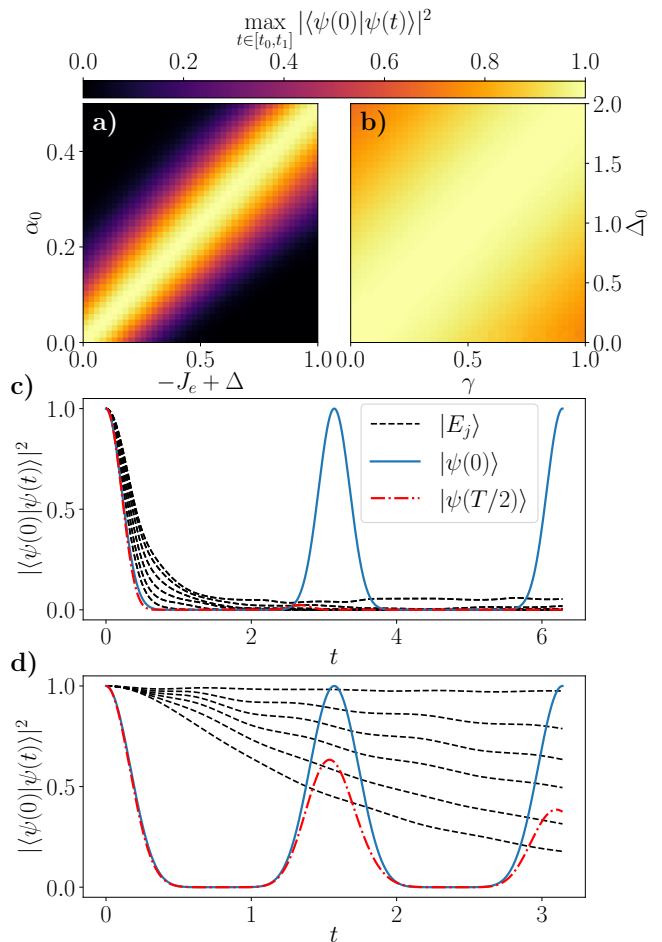


FIG. 2. (a) Maximum fidelity revival (between times $t_0 = 1$ and $t_1 = 2\pi$) for the driven SSH model in Eq. (13) with $\alpha(t) = -\alpha_0 \sin(2J_o t)$. The system size $N = 80$ and coupling $J_e = 2/3$ are fixed, while α_0 and Δ are varied. (b) Maximum fidelity revival (between $t_0 = 0.5$ and $t_1 = \pi$) for the driven AKLT model, Eq. (17), with $\Delta(t) = \Delta_0 \sin(\epsilon t)$. Data is for the system size $N = 50$, varying Δ_0 and γ . In both (a)-(b), data is obtained using numerical implementation of TDVP with bond dimension $\chi = 64$. (c)-(d): The scarred eigenstates $|E_j\rangle$ are destroyed by the Floquet operator, only the periodic orbit $|\psi(0)\rangle$ is preserved. Also shown is the periodic orbit shifted by $T/2$. Panel (c) is for the driven SSH model with system size $N = 22$, while panel (d) is for the driven AKLT model with system size $N = 12$. Data in both panels is obtained via exact diagonalization.

$J_e = 0$ model.

Suppose we modify the SSH chain by adding longer range hopping terms of the form:

$$\hat{\mathcal{H}} = \sum_n J_o \sigma_{2n+1}^+ \sigma_{2n+2}^- + J_e \sigma_{2n+2}^+ \sigma_{2n+3}^- + \Delta \sigma_{2n+1}^+ \sigma_{2n+4}^- + i\alpha(-1)^n (\sigma_{2n+1}^+ \sigma_{2n+3}^- - \sigma_{2n+2}^+ \sigma_{2n+4}^-) + \text{h.c.} \quad (13)$$

The additional hopping terms introduced here all satisfy Eqs. (5)-(6) and therefore Eq. (13) defines a class of models that share the same semiclassical limit as the

SSH chain. This form was chosen so the $\hat{\mathcal{H}}_1$ contributions all take $|\psi(t)\rangle$ to the same state. For this reason the quantum leakage takes a simple form,

$$\Gamma = \frac{\sqrt{N-2}}{T} \int_{t=0}^{T=\frac{\pi}{\epsilon}} \left| \frac{J_e + \Delta}{2} \sin(2J_o t) + \alpha \right| dt. \quad (14)$$

When $\Gamma = 0$, the periodic TDVP trajectory becomes an exact trajectory in the full quantum dynamics. By fixing $\alpha = 0$ and $J_e = -\Delta$, we obtain a family of static Hamiltonians, Eq. (13), that admit exact periodic orbits. However, we can also make Γ vanish if we allow the coupling to vary with time, $\alpha(t) = -\frac{1}{2}(J_e + \Delta) \sin(2J_o t)$, as confirmed in Fig. 2(a). The latter Floquet model hosts the same periodic orbit as the static SSH model. However, unlike the static case, the tower of QMBS eigenstates are not preserved by the Floquet operator, see Fig. 2(c). This is reminiscent of Rydberg atoms with a modulated chemical potential [12], where the scarred initial state also has high overlap with only a few Floquet modes [44].

AKLT model.—Our construction can also embed trajectories that involve entangled states with non-trivial correlations. As a second example, we consider the AKLT model [45]:

$$\hat{\mathcal{H}}_{\text{AKLT}} = \sum_n \mathbf{S}_n \cdot \mathbf{S}_{n+1} + \frac{1}{3} (\mathbf{S}_n \cdot \mathbf{S}_{n+1})^2, \quad (15)$$

where \mathbf{S}_n is a spin-1 operator on lattice site n . The AKLT model features a tower of QMBS states, generated by repeatedly applying the π -momentum spin-raising operator, $Q^+ = \sum_n (-1)^n (S_n^+)^2$, to the ground state [8, 46]. In Ref. [21], a $\chi=4$ MPS initial state which periodically oscillates was identified by applying a $\chi=2$ matrix-product operator to the AKLT ground state. Here we instead use the following $\chi=2$ initial state,

$$|\psi(0)\rangle = \bigotimes_n (\mathbb{1} + (-1)^n (S_n^+)^2 / 2) |\psi_{\text{GS}}^{\text{AKLT}}\rangle, \quad (16)$$

This state oscillates periodically at constant entanglement entropy $S_E(t) = \log(2)$, with the period set by the level spacing in the scarred subspace, $\epsilon=4$. We construct $\hat{\mathcal{H}}_1$ which satisfies Eqs. (5)-(6) by noting that for the AKLT ground state, no two neighboring sites can be in the state $|-\rangle$, a property inherited by $|\psi(t)\rangle$. As $P_{\mathcal{T}}$ differs from the MPS state $|\psi(t)\rangle$ on a single site, $\hat{\mathcal{H}}_1$ will satisfy Eq. (6) provided it maps at least four neighboring sites to $|-\rangle$. Therefore, introducing the state $|\chi_{-}\rangle \equiv |-, -, -, -\rangle$, a suitable Hamiltonian will be of the form $\hat{\mathcal{H}}_1 = \gamma \sum |\Phi\rangle \langle \chi_{-}| + \text{h.c.}$, where $|\Phi\rangle$ is an arbitrary state on four sites, which needs to have a finite overlap with $|\psi(t)\rangle$ in order to satisfy Eq. (5). These perturbations to the AKLT model differ fundamentally from those that preserve the entire tower of QMBS eigenstates in Ref. [21]. Indeed, the QMBS eigenstates of the AKLT model are not contained within the manifold, therefore

even perturbations with a perfectly coherent scarred orbit are not required to preserve the eigenstates.

Using quantum leakage, we can construct a driven perturbation of the AKLT model with an exact Floquet scarred state. First, we introduce the local basis vectors, $|\alpha_{\pm}\rangle = (|+\rangle \pm |-\rangle) / \sqrt{2}$. Using this basis, we examine the following two-parameter perturbation:

$$\begin{aligned} \hat{\mathcal{H}}_1 = & \sum_n \gamma |\alpha_+, \alpha_-, \alpha_+, \alpha_-\rangle \langle \chi_{-}| \\ & + \gamma |\alpha_-, \alpha_+, \alpha_-, \alpha_+\rangle \langle \chi_{-}| \\ & + (-1)^n \Delta |0, +, 0, +\rangle \langle \chi_{-}| + \text{h.c.} \end{aligned} \quad (17)$$

All of the terms in this $\hat{\mathcal{H}}_1$ map $|\psi(t)\rangle$ to the same state, therefore the leakage takes the form:

$$\Gamma \propto \sqrt{N} \int_{t=0}^{T=\frac{\pi}{\epsilon}} |\gamma \cos(\epsilon t) - \Delta/2| dt. \quad (18)$$

The leakage can be exactly cancelled by setting $\Delta = 2\gamma \cos(\epsilon t)$, as confirmed in Fig. 2(b). The Floquet model once again destroys the underlying tower of QMBS states, as shown in Fig. 2(d).

Conclusions and discussion.—We have presented a method for constructing classes of quantum Hamiltonians with equivalent semiclassical dynamics. This construction results in models that possess approximate QMBS associated with a semiclassical trajectory, reminiscent of scars in quantum billiards [25]. For the choice of Hamiltonians above, the calculation of the quantum leakage is tractable, allowing to write down new Floquet models with exact QMBSs (further examples of models that are amenable to our approach are presented in [43]). The choice of MPS states for defining the manifold \mathcal{M} was due to many QMBS models previously studied in the literature using MPS methods. However, our approach can be extended to other classes of variational wave functions such as bosonic or fermionic Gaussian states [47] or projected entangled pair states (PEPS) [42].

The approach here complements recent works which construct exact Floquet QMBSs using classical cellular automata [48, 49]. In particular, it furnishes a constructive realization of orbit “steering” based on quantum leakage by Ljubotina *et al.* [50]. In contrast to the latter, our approach yields exact Floquet QMBSs without the need for variational optimization. Furthermore, it should be pointed out that our method does not require that the periodic orbit be generated by QMBS, e.g., it could result from other ergodicity-breaking mechanisms, such as integrability or Hilbert space fragmentation.

If the states in \mathcal{M} form an overcomplete basis, then a Feynman path integral over the manifold can be constructed [41]. The saddle point equations of the path integral will correspond to the TDVP equations of motion, while additional perturbative corrections eventually reproduce the exact quantum dynamics. In particular, the quadratic corrections to TDVP equations of motion can be related to Lyapunov exponents which characterise the

chaotic nature of mixed semiclassical phase space [33, 51]. For Hamiltonians which can be decomposed in the manner introduced in this paper, it is possible to write analytic expressions for the Lyapunov exponents [52].

In some physical applications, one would wish to “invert” the above procedure, i.e., given a manifold \mathcal{M} and a Hamiltonian $\hat{\mathcal{H}}$, describing some physical system which supports QMBS, one would like to identify a decomposition into $\hat{\mathcal{H}}_0$ and $\hat{\mathcal{H}}_1$, such that Eqs. (4)-(6) approximately hold. A notable example is the PXP model [53, 54], which provides an effective description of QMBS in Rydberg atom arrays. In the PXP model, it is not obvious how to perform the decomposition into $\hat{\mathcal{H}}_0$ and $\hat{\mathcal{H}}_1$, although it has been conjectured that a suitable deformation of the model could result in exact QMBS [30, 55, 56]. In this context, we note that, while Eq. (10) or Eq. (11) are sufficient conditions to satisfy Eq. (6), they are not necessary. Hence, it would be interesting to understand if there exist more general yet analytically tractable mechanisms for embedding periodic orbits into larger families of non-integrable quantum Hamiltonians.

Acknowledgments.—We acknowledge support by EPSRC grant EP/R513258/1 and by the Leverhulme Trust Research Leadership Award RL-2019-015. Statement of compliance with EPSRC policy framework on research data: This publication is theoretical work that does not require supporting research data.

-
- [1] J. M. Deutsch, *Phys. Rev. A* **43**, 2046 (1991).
 [2] M. Srednicki, *Phys. Rev. E* **50**, 888 (1994).
 [3] M. Serbyn, D. A. Abanin, and Z. Papić, *Nature Physics* **17**, 675 (2021).
 [4] S. Moudgalya, B. A. Bernevig, and N. Regnault, *Reports on Progress in Physics* **85**, 086501 (2022).
 [5] A. Chandran, T. Iadecola, V. Khemani, and R. Moessner, arXiv e-print (2022), arXiv:2206.11528.
 [6] I. Affleck, T. Kennedy, E. H. Lieb, and H. Tasaki, *Phys. Rev. Lett.* **59**, 799 (1987).
 [7] D. P. Arovas, *Physics Letters A* **137**, 431 (1989).
 [8] S. Moudgalya, N. Regnault, and B. A. Bernevig, *Phys. Rev. B* **98**, 235156 (2018).
 [9] C. J. Turner, A. A. Michailidis, D. A. Abanin, M. Serbyn, and Z. Papić, *Nat. Phys.* **14**, 745 (2018).
 [10] C. J. Turner, A. A. Michailidis, D. A. Abanin, M. Serbyn, and Z. Papić, *Phys. Rev. B* **98**, 155134 (2018).
 [11] H. Bernien, S. Schwartz, A. Keesling, H. Levine, A. Omran, H. Pichler, S. Choi, A. S. Zibrov, M. Endres, M. Greiner, V. Vuletić, and M. D. Lukin, *Nature* **551**, 579 (2017).
 [12] D. Bluvstein, A. Omran, H. Levine, A. Keesling, G. Semeghini, S. Ebadi, T. T. Wang, A. A. Michailidis, N. Maskara, W. W. Ho, S. Choi, M. Serbyn, M. Greiner, V. Vuletić, and M. D. Lukin, *Science* **371**, 1355 (2021).
 [13] S. Dooley, *PRX Quantum* **2**, 020330 (2021).
 [14] J.-Y. Desaulles, F. Pietracaprina, Z. Papić, J. Goold, and S. Pappalardi, *Phys. Rev. Lett.* **129**, 020601 (2022).
 [15] S. Dooley, S. Pappalardi, and J. Goold, *Phys. Rev. B* **107**, 035123 (2023).
 [16] P. N. Jepsen, Y. K. E. Lee, H. Lin, I. Dimitrova, Y. Margalit, W. W. Ho, and W. Ketterle, *Nature Physics* **18**, 899 (2022).
 [17] G.-X. Su, H. Sun, A. Hudomal, J.-Y. Desaulles, Z.-Y. Zhou, B. Yang, J. C. Halimeh, Z.-S. Yuan, Z. Papić, and J.-W. Pan, arXiv e-print (2022), arXiv:2201.00821.
 [18] P. Zhang, H. Dong, Y. Gao, L. Zhao, J. Hao, J.-Y. Desaulles, Q. Guo, J. Chen, J. Deng, B. Liu, W. Ren, Y. Yao, X. Zhang, S. Xu, K. Wang, F. Jin, X. Zhu, B. Zhang, H. Li, C. Song, Z. Wang, F. Liu, Z. Papić, L. Ying, H. Wang, and Y.-C. Lai, *Nature Physics* (2022).
 [19] N. Shiraishi and T. Mori, *Phys. Rev. Lett.* **119**, 030601 (2017).
 [20] T. Iadecola, M. Schechter, and S. Xu, *Phys. Rev. B* **100**, 184312 (2019).
 [21] D. K. Mark, C.-J. Lin, and O. I. Motrunich, *Phys. Rev. B* **101**, 195131 (2020).
 [22] N. O’Dea, F. Burnell, A. Chandran, and V. Khemani, *Phys. Rev. Research* **2**, 043305 (2020).
 [23] K. Pakrouski, P. N. Pallegar, F. K. Popov, and I. R. Klebanov, *Phys. Rev. Lett.* **125**, 230602 (2020).
 [24] S. Moudgalya and O. I. Motrunich, arXiv e-print (2022), arXiv:2209.03377.
 [25] E. J. Heller, *Phys. Rev. Lett.* **53**, 1515 (1984).
 [26] E. J. Heller, in *Chaos and quantum physics*, Vol. 52 (North-Holland: Amsterdam, 1991).
 [27] E. Bogomolny, *Physica D: Nonlinear Phenomena* **31**, 169 (1988).
 [28] M. V. Berry, *Proceedings of the Royal Society of London. Series A, Mathematical and Physical Sciences* **423**, 219 (1989).
 [29] C.-J. Lin and O. I. Motrunich, *Phys. Rev. Lett.* **122**, 173401 (2019).
 [30] S. Choi, C. J. Turner, H. Pichler, W. W. Ho, A. A. Michailidis, Z. Papić, M. Serbyn, M. D. Lukin, and D. A. Abanin, *Phys. Rev. Lett.* **122**, 220603 (2019).
 [31] K. Bull, J.-Y. Desaulles, and Z. Papić, *Phys. Rev. B* **101**, 165139 (2020).
 [32] W. W. Ho, S. Choi, H. Pichler, and M. D. Lukin, *Phys. Rev. Lett.* **122**, 040603 (2019).
 [33] A. A. Michailidis, C. J. Turner, Z. Papić, D. A. Abanin, and M. Serbyn, *Phys. Rev. X* **10**, 011055 (2020).
 [34] W. P. Su, J. R. Schrieffer, and A. J. Heeger, *Phys. Rev. Lett.* **42**, 1698 (1979).
 [35] P. A. M. Dirac, *Mathematical Proceedings of the Cambridge Philosophical Society* **26**, 376 (1930).
 [36] P. Kramer and M. Saraceno, *Geometry of the Time-Dependent Variational Principle in Quantum Mechanics*, Lecture Notes in Physics (Springer Berlin Heidelberg, 1981).
 [37] J. Haegeman, J. I. Cirac, T. J. Osborne, I. Pižorn, H. Verschelde, and F. Verstraete, *Phys. Rev. Lett.* **107**, 070601 (2011).
 [38] D. Pérez-García, F. Verstraete, M. M. Wolf, and J. I. Cirac, *Quantum Inf. Comput.* **7**, 401 (2007).
 [39] D. Huybrechts, *Complex Geometry: An Introduction*, Universitext (Berlin. Print) (Springer, 2005).
 [40] J. Haegeman, M. Mariën, T. J. Osborne, and F. Verstraete, *Journal of Mathematical Physics* **55**, 021902 (2014).
 [41] A. G. Green, C. A. Hooley, J. Keeling, and S. H. Simon,

Feynman path integrals over entangled states (2016).

- [42] J. I. Cirac, D. Pérez-García, N. Schuch, and F. Verstraete, *Rev. Mod. Phys.* **93**, 045003 (2021).
- [43] See the Supplemental Material for background calculations and additional examples that support the results in the main text. The supplementary material contains Refs. [57, 58].
- [44] A. Hudomal, J.-Y. Desaulès, B. Mukherjee, G.-X. Su, J. C. Halimeh, and Z. Papić, *Phys. Rev. B* **106**, 104302 (2022).
- [45] I. Affleck, T. Kennedy, E. H. Lieb, and H. Tasaki, *Phys. Rev. Lett.* **59**, 799 (1987).
- [46] S. Moudgalya, S. Rachel, B. A. Bernevig, and N. Regnault, *Phys. Rev. B* **98**, 235155 (2018).
- [47] T. Guaita, L. Hackl, T. Shi, C. Hubig, E. Demler, and J. I. Cirac, *Phys. Rev. B* **100**, 094529 (2019).
- [48] T. Iadecola and S. Vijay, *Phys. Rev. B* **102**, 180302 (2020).
- [49] P.-G. Rozon, M. J. Gullans, and K. Agarwal, *Phys. Rev. B* **106**, 184304 (2022).
- [50] M. Ljubotina, B. Roos, D. A. Abanin, and M. Serbyn, *PRX Quantum* **3**, 030343 (2022).
- [51] A. Hallam, J. G. Morley, and A. G. Green, *Nature Communications* **10**, 2708 (2019).
- [52] Hallam *et al.* (2023), in preparation.
- [53] P. Fendley, K. Sengupta, and S. Sachdev, *Phys. Rev. B* **69**, 075106 (2004).
- [54] I. Lesanovsky and H. Katsura, *Phys. Rev. A* **86**, 041601(R) (2012).
- [55] V. Khemani, C. R. Laumann, and A. Chandran, *Phys. Rev. B* **99**, 161101(R) (2019).
- [56] K. Omiya and M. Müller, *Phys. Rev. A* **107**, 023318 (2023).
- [57] M. Schecter and T. Iadecola, *Phys. Rev. Lett.* **123**, 147201 (2019).
- [58] T. Iadecola and M. Schecter, *Phys. Rev. B* **101**, 024306 (2020).

Supplemental Online Material for “Embedding semiclassical periodic orbits into chaotic many-body Hamiltonians”

Andrew Hallam¹, Jean-Yves Desaulles¹, and Zlatko Papić¹
School of Physics and Astronomy, University of Leeds, Leeds LS2 9JT, UK

In this Supplementary Material, we derive the conditions for the embedding of a periodic orbit in cases where the variational manifold is spanned by matrix product states. We also provide details of the quantum leakage computation for the Su-Schrieffer-Heeger (SSH) model and Affleck-Kennedy-Lieb-Tasaki (AKLT) model discussed in the main text. Finally, we illustrate that our approach can be applied to other scarred models, such as the spin-1 XY model from Ref. [57] and a model with the emergent kinetic constraint from Ref. [58].

SUFFICIENT CONDITIONS FOR A TDVP PERIODIC ORBIT IN THE MPS MANIFOLD

In this section we prove the sufficient conditions that the MPS transfer matrix, and thereby perturbation $\hat{\mathcal{H}}_1$, need to obey in order to sustain a periodic orbit in the TDVP manifold. We assume the perturbing Hamiltonian is a tensor product of local operators,

$$\hat{\mathcal{H}}_1 = \sum_n \bigotimes_{k=1}^{2K} \hat{O}_k^{n+k-1}, \quad (\text{S1})$$

and denote the MPS transfer matrices as

$$\mathbb{E}_n(\hat{O}_k) = \sum_{s, \bar{s}'} \bar{A}_n^{s'} \hat{O}_{k,s, \bar{s}'}^n A_n^s. \quad (\text{S2})$$

Working on a finite spin chain with open boundary conditions, we parametrize the MPS tangent space in the following way:

$$|\partial_{A^n} \psi\rangle \rightarrow \sum_n \sum_{\{\sigma_n\}} (\dots A^{n-1} B^n A^{n+1} \dots) |\dots \sigma_{n-1} \sigma_n \sigma_{n+1} \dots\rangle. \quad (\text{S3})$$

For the sake of this discussion, B^n is not required to take any particular form. We also introduce the environment of the tensor network contracted from the left and right, respectively,

$$|\mathbb{L}_n\rangle = \prod_{m=1}^n \mathbb{E}_0^m, \quad |\mathbb{R}_n\rangle = \prod_{m=n}^N \mathbb{E}_0^m, \quad (\text{S4})$$

where \mathbb{E}_n^0 is a shorthand notation for $\mathbb{E}_n(\mathbb{1})$. Finally, let us introduce the mixed MPS transfer matrix

$$\mathbb{E}_n^{\bar{B}}(\hat{O}_k) = \sum_{s, \bar{s}'} \bar{B}_n^{s'} O_{k,s, \bar{s}'}^n A_n^s, \quad (\text{S5})$$

with $\mathbb{E}_n^{\bar{B},0}$ representing the case $O = \mathbb{1}$. Using these expressions, we can show that $\langle \partial_{A^n} \psi | \hat{\mathcal{H}}_1 | \psi \rangle = 0$ provided that

$$\prod_{k=1}^K \mathbb{E}_{n+k-1}(\hat{O}_k) = 0, \quad \prod_{k=K+1}^{2K} \mathbb{E}_{n+k-1}(\hat{O}_k) = 0. \quad (\text{S6})$$

In order to demonstrate this let us analyze the various possible cases in turn. Firstly, when the Hamiltonian is one of $2K$ sites that do not overlap with the tangent vector MPS, we find contributions like

$$|\mathbb{L}_{n-1}\rangle \left(\prod_{k=1}^{2K} \mathbb{E}_{n+k-1}(\hat{O}_k) \right) \left(\prod_{j=n+2K}^{j'-1} \mathbb{E}_n^0 \right) \mathbb{E}_{j'}^{\bar{B},0} |\mathbb{R}_{j'+1}\rangle, \quad (\text{S7})$$

which is clearly zero if $\prod_{k=1}^K \mathbb{E}_{n+k-1}(\hat{O}_k) = 0$ or $\mathbb{E}_{n+k-1}(\hat{O}_k) = 0$. When the tangent vector is located to the left of the Hamiltonian, the contributions will similarly be zero. When the tangent vector overlaps with the Hamiltonian, we will find contributions like

$$\langle \mathbb{L}_{n-1} | \left(\prod_{k=1}^{k'-1} \mathbb{E}_{n+k-1}(\hat{O}_k) \right) \mathbb{E}_{n+k'-1}^{\hat{B}}(\hat{O}_{k'}) \left(\prod_{k=k'+1}^{2K} \mathbb{E}_{n+k-1}(\hat{O}_k) \right) | \mathbb{R}_{n+2K} \rangle. \quad (\text{S8})$$

Since the tangent vector will be in either the first half or the second half of the Hamiltonian, either $\prod_{k=1}^K \mathbb{E}_{n+k-1}(\hat{O}_k) = 0$ or $\mathbb{E}_{n+k-1}(\hat{O}_k) = 0$ will force this contribution to be zero. These contributions are zero regardless of the particular form of $\langle \mathbb{L}_n |$ and $| \mathbb{R}_n \rangle$, for this reason they also apply naturally to MPS with periodic boundary conditions. If we work in the thermodynamic limit, with a translation invariant, injective MPS tensor A^s , the MPS transfer matrix will have a dominant left and right eigenvectors with eigenvalue $\lambda = 1$,

$$\langle \mathbb{L} | \mathbb{E}_0 = \langle \mathbb{L} |, \quad \mathbb{E}_0 | \mathbb{R} \rangle = | \mathbb{R} \rangle. \quad (\text{S9})$$

The equations equivalent to Eqs. (S7)-(S8) now begin and end with the same eigenvectors everywhere, $\langle \mathbb{L} |$ and $| \mathbb{R} \rangle$. Therefore, the conditions for $\langle \partial_{A^n} \psi | \hat{\mathcal{H}}_1 | \psi \rangle = 0$ can be weakened to

$$\langle \mathbb{L} | \prod_{k=1}^K \mathbb{E}_{n+k-1}(\hat{O}_k) = 0, \quad \prod_{k=K+1}^{2K} \mathbb{E}_{n+k-1}(\hat{O}_k) | \mathbb{R} \rangle = 0, \quad (\text{S10})$$

as stated in the main text. This condition can be easily generalized to an n -site translation invariant MPS in the thermodynamic limit.

SSH MODEL: LEAKAGE CALCULATION

In the main text we considered a modified SSH model on a N -site chain with open boundary conditions (OBC). We can divide the model up into $\hat{\mathcal{H}}_0$ and $\hat{\mathcal{H}}_1$ terms, where $\hat{\mathcal{H}}_0$ takes the form

$$\hat{\mathcal{H}}_0 = \sum_{n=0}^{N/2-1} J_o \sigma_{2n+1}^+ \sigma_{2n+2}^- + \text{h.c.} \quad (\text{S11})$$

For this Hamiltonian, the initial state $|\psi(0)\rangle = \bigotimes_{n=0}^{n=N/4-1} |1, 0, 0, 1\rangle$ oscillates periodically, taking the form

$$|\psi(t)\rangle = \bigotimes_{n=0}^{N/4-1} |\phi_1(t)\rangle \otimes |\phi_2(t)\rangle = \bigotimes_n (\cos(J_o t) |01\rangle - i \sin(J_o t) |10\rangle) \otimes (\cos(J_o t) |10\rangle - i \sin(J_o t) |01\rangle), \quad (\text{S12})$$

where $|\phi_1(t)\rangle$ is the same for every pair of sites $\{4n+1, 4n+2\}$ and, similarly, $|\phi_2(t)\rangle$ is on sites $\{4n+3, 4n+4\}$. For this reason, it is appropriate to block together sites $\{4n+1, 4n+2\}$ and $\{4n+3, 4n+4\}$. This $d=4$, $\chi=1$ MPS ansatz defines the variational manifold for which we calculate the TDVP equations and quantum leakage.

Given this, we can choose the $\hat{\mathcal{H}}_1$ Hamiltonian to be,

$$\hat{\mathcal{H}}_1 = \sum_{n=0}^{N/2-2} J_e \sigma_{2n+2}^+ \sigma_{2n+3}^- + \Delta \sigma_{2n+1}^+ \sigma_{2n+4}^- + i\alpha (-1)^n (\sigma_{2n+2}^+ \sigma_{2n+4}^- - \sigma_{2n+1}^+ \sigma_{2n+3}^-) + \text{h.c.} \quad (\text{S13})$$

We find that the instantaneous quantum leakage is

$$\Gamma(t) = \| \hat{\mathcal{H}}_1 | \psi(t) \rangle \|. \quad (\text{S14})$$

We can evaluate this by calculating the action one term of $\hat{\mathcal{H}}_1$ on $|\psi(t)\rangle$. A single term of $\hat{\mathcal{H}}_1$ acting on $|\phi_1(t)\rangle \otimes |\phi_2(t)\rangle$ in $|\psi(t)\rangle$ is

$$\left(\bigotimes |\phi_1(t)\rangle \otimes |\phi_2(t)\rangle \right) \otimes (-i((J_e + \Delta) \cos(J_o t) \sin(J_o t) + \alpha) (|0011\rangle + |1100\rangle)) \left(\bigotimes |\phi_1(t)\rangle \otimes |\phi_2(t)\rangle \right). \quad (\text{S15})$$

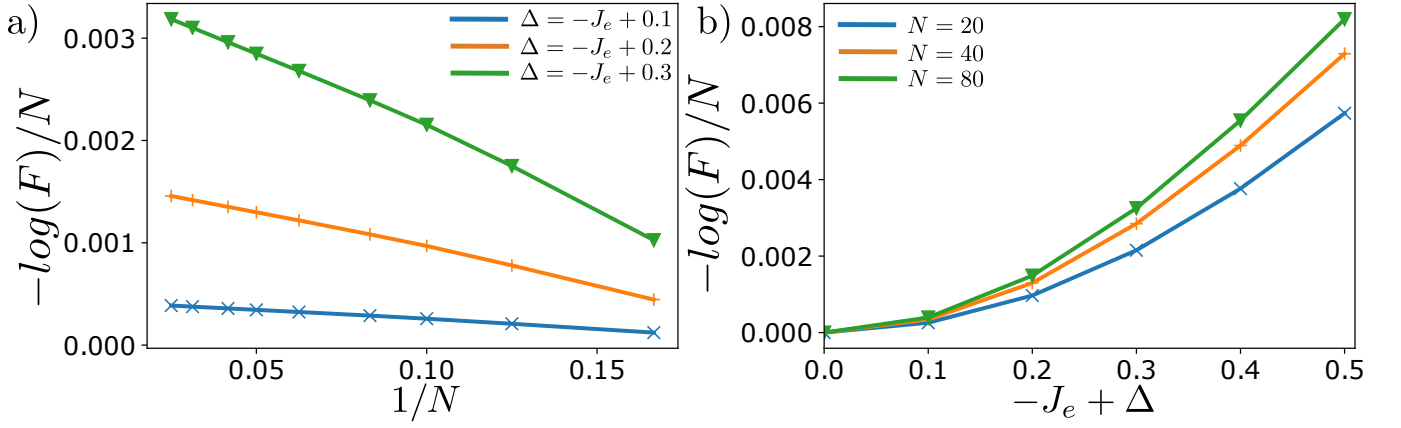


FIG. S1. $-\log(F)/N$ for the SSH model with $J_o = 1$, $J_e = 2/3$, $\alpha = 0$ and varying Δ . a) shows $-\log(F)/N$ against $1/N$ for various Δ , it approaches a value far from $\log(2)$ in the thermodynamic limit, indicating strong revivals. b) shows $-\log(F)/N$ for various N as a function of Δ , it appears to grow approximately quadratically.

A similar result is obtained when $\hat{\mathcal{H}}_1$ acts on $|\phi_2(t)\rangle \otimes |\phi_1(t)\rangle$ instead. So in total there are $N/2 - 1$ terms in $\hat{\mathcal{H}}_1$, all of which have zero overlap with one another and contribute similarly. For this reason, we find that the total instantaneous quantum leakage is

$$\begin{aligned}
 \Gamma(t) &= \left\| \sum_{n=0}^{N/2-2} |\psi_{L,2n}(t)\rangle \otimes (|0011\rangle + |1100\rangle) \otimes |\psi_{R,2n+5}(t)\rangle \right\| \times |(J_e + \Delta) \cos(J_o t) \sin(J_o t) + \alpha| \\
 &= \sqrt{N/2 - 1} \times \sqrt{2} \times \left| \frac{1}{2} (J_e + \Delta) \sin(2J_o t) + \alpha \right| \\
 &= \sqrt{N - 2} \times \left| \frac{1}{2} (J_e + \Delta) \sin(2J_o t) + \alpha \right|, \tag{S16}
 \end{aligned}$$

where $|\psi_{L,2n}(t)\rangle$ and $|\psi_{R,2n+5}(t)\rangle$ denote the parts of $|\psi(t)\rangle$ on which the term of $\hat{\mathcal{H}}_1$ is not acting, and which is simply composed of a tensor product of $|\phi_1(t)\rangle$ and $|\phi_2(t)\rangle$. When the leakage does not exactly cancel, quantum dynamics will only approximately be periodic. We characterize such approximate periodic dynamics using the maximum fidelity revival, $F = \max_{t \in [t_1, t_2]} |\langle \psi(t) | \psi(t=0) \rangle|^2$, over some moderate time interval $[t_1, t_2]$ that exceeds an initial relaxation (given by the energy scales of the microscopic Hamiltonian). For a generic quantum trajectory, the fidelity density $-\log(F)/N$ is expected to approach $\log(d)$ in the thermodynamic limit, where d is the local Hilbert space dimension on each site. In Fig. (S1)(a), we see that the fidelity density remains small for various Δ as the system size increases. Moreover, in Fig. (S1)(b), we see $-\log(F)/N$ has an approximately quadratic dependence on $-J_e + \Delta$.

We note that the same results hold for periodic boundary conditions as long as N is a multiple of 4. The only difference is that the prefactor in the leakage becomes \sqrt{N} instead of $\sqrt{N-2}$.

Nearest-neighbor coupling

If, instead, $\hat{\mathcal{H}}_1$ contains next-next-nearest neighbor term of the form

$$\hat{\mathcal{H}}_1 = \sum_{n=0}^{N/2-2} J_e \sigma_{2n+2}^+ \sigma_{2n+3}^- + \Delta \sigma_{2n+1}^+ \sigma_{2n+4}^- + \sum_{n=0}^{N/2-3} J_{nn} \sigma_{2n+2}^+ \sigma_{2n+5}^- + h.c., \tag{S17}$$

we can once again perform the quantum leakage calculation. We find one contribution equivalent to the calculation in the previous section, with an additional term due to J_{nn} acting on next-nearest neighboring sites in the $d = 4$ ansatz. Taking into account these terms, we find that the instantaneous quantum leakage is

$$\Gamma(t) = \sqrt{N/2 - 1} \sqrt{1/2 (J_e + J_{nn})^2 \sin(2J_o t)^2 + J_{nn}^2 \frac{N/2 - 2}{N/2 - 1} (\sin(J_o t)^4 + \cos(J_o t)^4)}. \tag{S18}$$

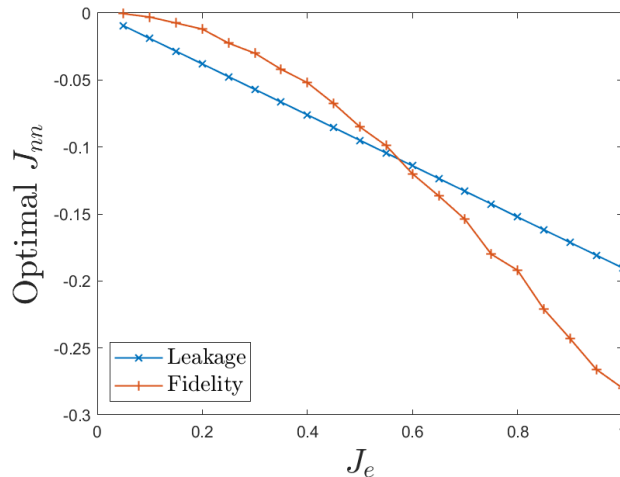


FIG. S2. The optimal value of J_{nn} that minimizes quantum leakage, found using Eq. (S18), with $J_o = 1$, $N = 50$ (blue). This can be compared with the maximum fidelity revival found numerically using $\chi = 64$ TDVP with a timestep of $\delta t = 0.025$ (orange).

As the two terms under the square root are both positive definite, it is clear that there is no choice of J_{nn} which will lead to $\Gamma(t) = 0$ for finite J_e . Nevertheless, increasing J_{nn} can still reduce the leakage. Fig. S2 shows the optimal choice of J_{nn} that minimizes the leakage. We see that the optimal J_{nn} increases linearly with J_e . This is in reasonably good agreement with the optimal choice of J_{nn} found by maximizing the fidelity revival for the exact quantum dynamics.

We note that, in addition to the nearest-neighbor coupling considered above, Ref. [18] also found that a driven perturbation of the form $\propto \sum_n \sin(\Omega t) \sigma_n^z$ can enhance the periodic revivals due to scarring. Unfortunately, it is not possible to treat such perturbations using the method introduced here, as any single-site operator commutes with the tangent space projector, therefore it is not of the appropriate form required for \mathcal{H}_1 .

SPIN-1 XY MODEL

Another model that has been rigorously shown to exhibit quantum many-body scars is the spin-1 XY chain [57],

$$\hat{\mathcal{H}}_0 = \sum_n J(S_n^x S_{n+1}^x + S_n^y S_{n+1}^y) + h S_n^z + D(S_n^z)^2. \quad (\text{S19})$$

Here, we will once again work with open-boundary conditions (OBC). This model features a tower of scarred eigenstates generated by repeatedly applying the operator

$$Q^+ = \sum_n (-1)^n (S_n^+)^2 \quad (\text{S20})$$

on the state $|0\rangle = \otimes_n |m_n = -1\rangle$. The m -th eigenstate in this tower has an energy $E_m = h(2m - N) + ND$. Due to the even level spacing of this tower, any state written as a superposition of these eigenstates will oscillate periodically. One particularly nice example is the initial state

$$|\psi(t=0)\rangle = \bigotimes_n \frac{1}{\sqrt{2}} (|m_n = -1\rangle + (-1)^n |m_n = 1\rangle), \quad (\text{S21})$$

for which $|\psi(t)\rangle$ remains an unentangled, product state throughout its evolution. Therefore its behavior is captured entirely by $d = 2$, $\chi = 1$ MPS.

We can choose

$$\hat{\mathcal{H}}_1 = \gamma \sum_n (S_n^x S_{n+1}^x - S_n^y S_{n+1}^y) + \sum_n (-1)^n \Delta (S_n^x S_{n+1}^y - S_n^y S_{n+1}^x) \quad (\text{S22})$$

to satisfy the conditions in Eq. (5) and Eq. (6) in the main text. $\hat{\mathcal{H}}_1$ will clearly satisfy Eq. (5) but Eq. (6) is more subtle. We can see Eq. (6) is satisfied by noting that every site in every state in the TDVP ansatz is some superposition of $m_i = -1$ or $m_i = 1$ and $\hat{\mathcal{H}}_1$ will flip two sites of the system to be $m_i = 0$. The tangent space projector is equal to $|\psi(t)\rangle$ on all but one site, but $\hat{\mathcal{H}}_1$ will make the state orthogonal to $|\psi(t)\rangle$ on two sites, therefore Eq. (6) of the main text will be satisfied.

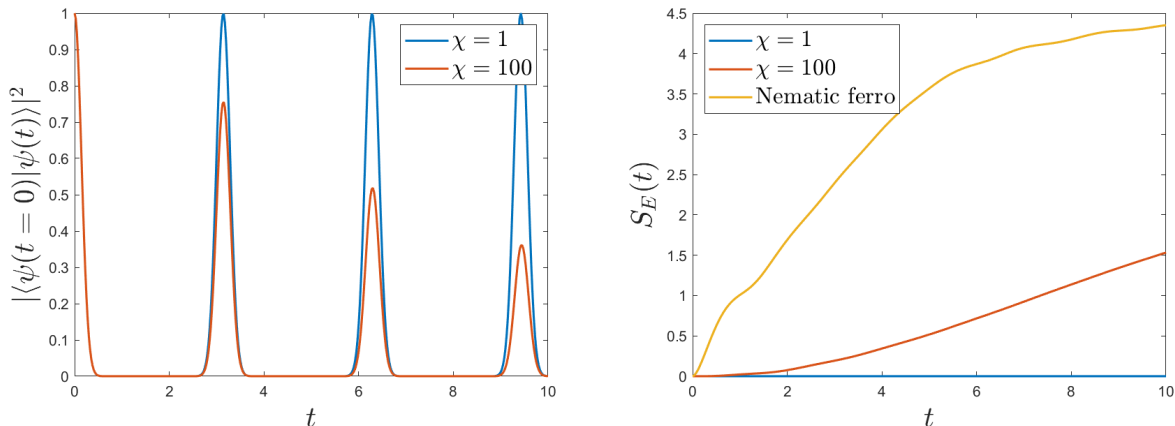


FIG. S3. Left: Fidelity revivals for the modified spin-1 XY model with $J = 1$, $h = 1$, $D = 0.5$, $\gamma = 0.1$, $\Delta = 0$, $L = 16$. Perfect fidelity revivals are seen for the TDVP ansatz ($\chi = 1$) compared to the full quantum evolution. Right: Entanglement entropy growth for the same model. The full dynamics still exhibits slow entropy growth compared to a generic state (“nematic ferro”).

In Fig. S3(a) we compute the fidelity revivals for the spin-1 XY model after introducing a perturbation with $\gamma = 0.1$, $\Delta = 0.0$, which destroys the exact scarring structure. For bond dimension $\chi = 1$ we have a product state ansatz and the revivals remain exact but the full quantum dynamics exhibits only imperfect revivals. Fig. S3(b) shows the entropy growth. The ansatz has exactly zero entropy for all times but the full dynamics still exhibits slow entropy growth compared to a generic initial state, the nematic ferromagnetic state $|\psi(t=0)\rangle = \bigotimes_i \frac{1}{\sqrt{2}}(|m_i = -1\rangle + |m_i = 1\rangle)$.

We find that the leakage in this case is

$$\Gamma = \frac{\sqrt{N-1}}{T} \int_0^T |\gamma \sin(2ht) - \Delta| dt. \quad (\text{S23})$$

Therefore, by choosing $\Delta = \gamma \sin(2ht)$, we can once again construct Floquet scars through exact cancellation of the quantum leakage. For this reason, we choose $\Delta = \delta \sin(2ht)$ and vary γ and δ . In Fig. S4 we show the behavior of the driven spin-1 XY model for various γ and δ . When $\gamma = \delta$ we see perfect fidelity revivals despite it being a strongly driven system. We see that the entropy growth is suppressed to near zero in Fig. S4(b). In Fig. S4(c) we show the integrated leakage (divided by system size), which closely predicts the behavior of the entropy and fidelity.

COMPUTATION OF LEAKAGE IN THE AKLT MODEL

As an example of a model whose periodic orbit features entangled states, in the main text we considered the spin-1 AKLT model:

$$\hat{\mathcal{H}}_{\text{AKLT}} = \sum_i \mathbf{S}_i \cdot \mathbf{S}_{i+1} + \frac{1}{3} (\mathbf{S}_i \cdot \mathbf{S}_{i+1})^2. \quad (\text{S24})$$

The AKLT model features a tower of scarred states generated by the same operator as the spin-1 XY model, although it now acts upon the entangled AKLT ground-state defined by the three MPS tensors

$$A^+ = \sqrt{\frac{2}{3}} \begin{pmatrix} 0 & 1 \\ 0 & 0 \end{pmatrix}, \quad A^0 = \sqrt{\frac{1}{3}} \begin{pmatrix} -1 & 0 \\ 0 & 1 \end{pmatrix}, \quad A^- = -\sqrt{\frac{2}{3}} \begin{pmatrix} 0 & 0 \\ 1 & 0 \end{pmatrix}. \quad (\text{S25})$$

In the case of open boundary conditions, the AKLT ground-state is four-fold degenerate. The tower of eigenstates are only generated by acting on one of these ground-states, chosen by applying the boundary vectors $v_L = (1, 0)$ and

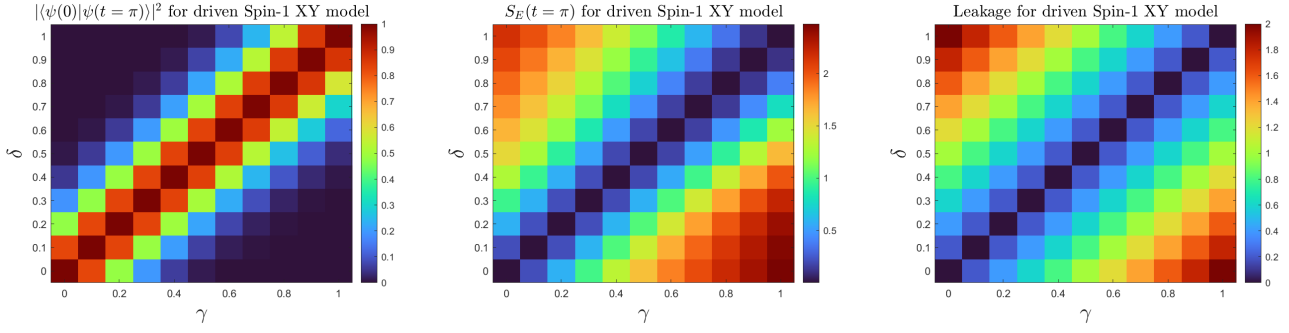


FIG. S4. Behavior of the driven spin-1 XY model for fixed $J = 1$, $h = 1$, $D = 0.5$ and $L = 16$ while varying δ and γ . Left: Fidelity revival at $t = \pi$. Middle: Entropy at $t = \pi$. Right: Integrated leakage rescaled by the square root of the system size Γ/\sqrt{N} .

$v_R = (0, 1)$ to the first and last sites of the system. We can find a bond-dimension two initial state

$$|\psi(t=0)\rangle = \bigotimes_j (\mathbb{1} + z(-1)^j (S_j^+)^2) |\psi_{\text{GS}}\rangle \quad (\text{S26})$$

which has overlap with only the scarred AKLT subspace. In fact, this state is the natural equivalent of the spin-1 XY initial state considered above. The dynamics from this initial state is remarkably simple:

$$|\psi(t)\rangle = \bigotimes_j (\mathbb{1} + z(-1)^j e^{i\epsilon t} (S_j^+)^2) |\psi_{\text{GS}}\rangle. \quad (\text{S27})$$

The state periodically oscillates, with the period set by the level spacing in the scarred subspace, $\epsilon = 4$. In terms of the MPS tensors this looks like:

$$A_j^+(t) = \sqrt{\frac{2}{3}} \begin{pmatrix} 0 & 1 \\ 2(-1)^j z e^{i\epsilon t} & 0 \end{pmatrix}, \quad A_j^0(t) = \sqrt{\frac{1}{3}} \begin{pmatrix} -1 & 0 \\ 0 & 1 \end{pmatrix}, \quad A_j^-(t) = -\sqrt{\frac{2}{3}} \begin{pmatrix} 0 & 0 \\ 1 & 0 \end{pmatrix}. \quad (\text{S28})$$

We can now focus on the case of an infinite chain. For that, we need to compute the two-site transfer matrix for this MPS tensor which is

$$\frac{1}{9} \begin{pmatrix} 5 + 16|z|^2 & 0 & 0 & 4 \\ 0 & 1 - 16|z|^2 & 0 & 0 \\ 0 & 0 & 1 - 16|z|^2 & 0 \\ 4(4|z|^2 + 1) & 0 & 0 & 5 + 16|z|^2 \end{pmatrix}, \quad (\text{S29})$$

with eigenvalues

$$\left\{ \frac{1}{9}(16|z|^2 + 4\sqrt{4|z|^2 + 1} + 5), \frac{1}{9}(16|z|^2 - 4\sqrt{4|z|^2 + 1} + 5), \frac{1}{9}(1 - 16|z|^2), \frac{1}{9}(1 - 16|z|^2) \right\}. \quad (\text{S30})$$

We therefore introduce a factor

$$\mathcal{N}(z) = \left(\frac{1}{9}(16|z|^2 + 4\sqrt{4|z|^2 + 1} + 5) \right)^{N/2} = \left(\frac{1}{3}(2\sqrt{4|z|^2 + 1} + 1) \right)^N = n_z^N, \quad (\text{S31})$$

which appropriately normalizes the state in the thermodynamic limit. Putting the MPS tensor into left canonical form, the dominant left/right eigenvectors become $|\mathbb{L}\rangle = \{1, 0, 0, 1\}$, $|\mathbb{R}\rangle = 1/2\{1, 0, 0, 1\}^T$, showing the state will evolve at constant entanglement entropy $S_E(t) = \log(2)$.

If we perform a local change of basis on every site, $|\alpha_{\pm}\rangle = \frac{1}{\sqrt{2}}(|+\rangle \pm |-\rangle)$, the time evolved state can be written

$$A_j^{\alpha+}(t) = \sqrt{\frac{1}{3}} \begin{pmatrix} 0 & 1 \\ -1 + 2(-1)^j z e^{i\epsilon t} & 0 \end{pmatrix}, \quad A_j^0(t) = \sqrt{\frac{1}{3}} \begin{pmatrix} -1 & 0 \\ 0 & 1 \end{pmatrix}, \quad A_j^{\alpha-}(t) = \sqrt{\frac{1}{3}} \begin{pmatrix} 0 & 1 \\ 1 + 2(-1)^j z e^{i\epsilon t} & 0 \end{pmatrix}. \quad (\text{S32})$$

By making the choice $z = 1/2$, the bottom left element of $A^{\alpha+}$ and $A^{\alpha-}$ can be rewritten respectively as $-2e^{i\epsilon t/2} \cos(\epsilon t/2)$ and $-2ie^{i\epsilon t/2} \sin(\epsilon t/2)$ for odd sites. For even sites they are $2ie^{i\epsilon t/2} \sin(\epsilon t/2)$ and $2e^{i\epsilon t/2} \cos(\epsilon t/2)$

respectively. For $z = 1/2$, $n_z = n_{1/2} = \frac{1}{3}(1 + 2\sqrt{2})$. Using this basis we can study the behavior of the following two parameter perturbation:

$$\hat{\mathcal{H}}_1 = \sum_i \gamma(|\alpha_+, \alpha_-, \alpha_+, \alpha_-\rangle \langle -, -, -, -| + |\alpha_-, \alpha_+, \alpha_-, \alpha_+\rangle \langle -, -, -, -|) + (-1)^i \Delta |0, +, 0, +\rangle \langle -, -, -, -| + h.c. \quad (\text{S33})$$

Calculating the leakage is more complicated in this case due to the non-zero overlap between $\hat{\mathcal{H}}_1$ acting on different sites. Let us write $\hat{\mathcal{H}}_1 = \sum_i h_i$. We first note that on the four sites where h_i modifies the MPS, the only nonzero basis vector is $|-\rangle$ and the product of the four MPS tensors is proportional to the identity, $h_i^{i,i+1,i+2,i+3} A^i A^{i+1} A^{i+2} A^{i+3} \propto \mathbb{1}_2$. Then we note that, $\langle \bar{\psi}(t) | h_i h_j | \psi(t) \rangle \neq 0$ only when $j = \{i-1, i, i+1\}$ due to $|\psi(t)\rangle$ not featuring two neighboring sites in the $|-\rangle$ state. Working in the thermodynamic limit, we can take each of these cases in turn, finding that

$$\begin{aligned} \langle \bar{\psi}(t) | h_i h_i | \psi(t) \rangle &= \frac{1}{81n_{1/2}^4} (\gamma(1 + e^{i\epsilon t})(1 + e^{i\epsilon t}) + \gamma(1 - e^{i\epsilon t})(1 - e^{i\epsilon t}) - 2\Delta e^{i\epsilon t}) \\ &\quad \times (\gamma(1 + e^{-i\epsilon t})(1 + e^{-i\epsilon t}) + \gamma(1 - e^{-i\epsilon t})(1 - e^{-i\epsilon t}) - 2\Delta e^{-i\epsilon t}) \\ &= \frac{1}{81n_{1/2}^4} (2\gamma(1 + e^{2i\epsilon t}) - 2\Delta e^{i\epsilon t}) (2\gamma(1 + e^{-2i\epsilon t}) - 2\Delta e^{-i\epsilon t}) \\ &= \frac{16}{81n_{1/2}^4} \left(\gamma \cos(\epsilon t) - \frac{\Delta}{2} \right)^2. \end{aligned} \quad (\text{S34})$$

For the other two cases, we find:

$$\langle \bar{\psi}(t) | h_i h_{i+1} | \psi(t) \rangle = \langle \bar{\psi}(t) | h_{i+1} h_i | \psi(t) \rangle = \frac{1}{3\sqrt{2}n_{1/2}} \langle \bar{\psi}(t) | h_i h_i | \psi(t) \rangle = \frac{16}{243\sqrt{2}n_{1/2}^5} \left(\gamma \cos(\epsilon t) - \frac{\Delta}{2} \right)^2. \quad (\text{S35})$$

Therefore, the quantum leakage in the thermodynamic limit is

$$\Gamma = \sqrt{N} \sqrt{\frac{16}{81n_{1/2}^4} + 2\frac{16}{243\sqrt{2}n_{1/2}^5}} \int_0^T \left| \gamma \cos(\epsilon t) - \frac{\Delta}{2} \right| dt = \frac{4\sqrt{N}}{9n_{1/2}^2} \sqrt{1 + \frac{\sqrt{2}}{3n_{1/2}}} \int_0^T \left| \gamma \cos(\epsilon t) - \frac{\Delta}{2} \right| dt. \quad (\text{S36})$$

For finite systems, the same arguments hold. So we get non-zero contributions that are still proportional to $|\gamma \cos(\epsilon t) - \frac{\Delta}{2}|$. This means that we can get a perfectly periodic orbit with the same driving parameters. However, the exact expression of Γ becomes non-trivial due to the normalization factor.

IADECOLA-SCHecter DOMAIN-WALL PRESERVING MODEL

Another model with a tower of scarred eigenstates that can be exactly constructed in the Iadecola-Schecter “domain-wall preserving” spin-1/2 model [58],

$$\hat{\mathcal{H}}_0 = \sum_n \lambda(\sigma_n^x - \sigma_{n-1}^z \sigma_n^x \sigma_{n+1}^z) + \Delta \sigma_n^z + J \sigma_n^z \sigma_{n+1}^z. \quad (\text{S37})$$

The tower of scarred states in this model is generated by the repeated application of the operator

$$Q^+ = \sum_n (-1)^n P_{n-1}^0 \sigma_n^+ P_{n+1}^0 \quad (\text{S38})$$

onto the state $\bigotimes_n |0\rangle$, where $P_n^0 = (1 - \sigma_n^z)/2$ is the projector onto spin down. These states have energies $E_n = (2\Delta - 4J)n + J(N - 1) - \Delta N$. While the model overall is unconstrained, the scarred eigenstates obey an emergent kinematic constraint in which no two neighboring sites can be occupied.

A simple state which exhibits periodic oscillations due to these scarred eigenstates is

$$|\eta\rangle \propto \mathcal{P}_c \prod_n [\mathbb{1} + (-1)^n \eta \sigma_n^+] |0\rangle \quad (\text{S39})$$

where $\mathcal{P}_c = \prod_n (1 - |11\rangle_{n,n+1} \langle 11|_{n,n+1})$ imposes the emergent kinematic constraint. This state can be written simply as a $\chi = 2, d = 2$ MPS where,

$$A^1 = (-1)^n \frac{\eta}{2} \begin{pmatrix} -1 & -1 \\ 1 & 1 \end{pmatrix}, \quad A^0 = \begin{pmatrix} 0 & 0 \\ -1 & 1 \end{pmatrix}. \quad (\text{S40})$$

Choosing $\chi = 2, d = 2$ for our variational manifold, it is straightforward to construct a valid $\hat{\mathcal{H}}_1$. If $\hat{\mathcal{H}}_1 |\psi(t)\rangle$ violates the emergent kinematic constraint in at least two places, the state will be annihilated by the tangent space projector. Therefore, it suffices to choose $\hat{\mathcal{H}}_1$ as

$$\hat{\mathcal{H}}_1 = \gamma \sum_n |\Phi\rangle \langle 1, 1, 1, 1| + \text{h.c.} \quad (\text{S41})$$

The construction of Floquet scars for this model is slightly more complicated than the previous examples. However, we can proceed if we notice that $A^0 A^0 = A^0$ and $A^0 A^1 A^0 = \eta(-1)^n A^0$. Using these relations and fixing $\eta = 1$, we introduce the following perturbation

$$\hat{\mathcal{H}}_1 = \sum_n \sigma_{n-3}^+ \sigma_{n-2}^+ [\gamma \sigma_{n-1}^+ P_n^1 \sigma_{n+1}^+ + \Delta (-1)^n (\sigma_{n-1}^+ \sigma_n^+ \sigma_{n+1}^+ + P_{n-1}^1 \sigma_n^+ P_{n+1}^1)] \sigma_{n+2}^+ \sigma_{n+2}^+ + \text{h.c.} \quad (\text{S42})$$

For this perturbation, we find that the instantaneous quantum leakage is proportional to

$$\Gamma \propto \int_0^T |\gamma + \frac{\Delta}{2} \cos(\epsilon t)| dt \quad (\text{S43})$$

and thus we obtain perfect Floquet scars when $\gamma = -2\Delta \cos(\epsilon t)$.